Chem Catalysis

Article

Stabilization of highly active Ru sites toward acidic water oxidation by dual-atom doping

Graphical abstract

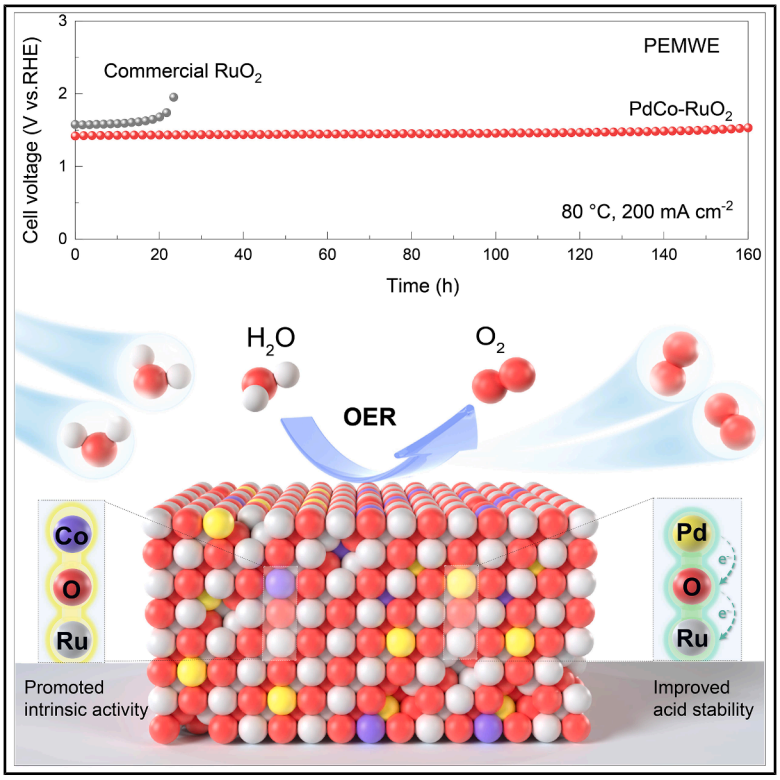

Highlights

- Atomic Co promotes OOH* deprotonation within local Co-O-Ru configuration
- Electron transfer occurs from Pd to Ru to suppress over-oxidation and dissolution
- Incorporation of Co and Pd into RuO_2 results in an active and stable PEMWE

Authors

Jialin Tang, Qisheng Zeng, Qiu Jiang, ..., Chih-Wen Pao, Xinyan Liu, Chuan Xia

Correspondence

pao.cw@nsrrc.org.tw (C.-W.P.), xinyanl@uestc.edu.cn (X.L.), chuan.xia@uestc.edu.cn (C.X.)

In brief

Ruthenium dioxide (RuO_2) shows great potential in the oxygen evolution reaction (OER) within proton exchange membrane water electrolyzers (PEMWEs). However, achieving an optimal balance between catalytic activity and acid stability remains a critical challenge. Here, we propose a Pd and Co co-doping strategy to enhance both the activity and stability of RuO_2 for the acidic OER. Co doping improves intrinsic catalytic activity by promoting OOH* deprotonation. Concurrently, Pd doping enhances the acid stability of Ru active sites, suppressing over-oxidation and dissolution.

Tang et al., 2025, Chem Catalysis *5*, 101441
October 16, 2025
https://doi.org/10.1016/j.checat.2025.101441

CellPress

Please cite this article in press as: Tang et al., Stabilization of highly active Ru sites toward acidic water oxidation by dual-atom doping, Chem Catalysis (2025), https://doi.org/10.1016/j.checat.2025.101441

Chem Catalysis

CellPress

Article

Stabilization of highly active Ru sites toward acidic water oxidation by dual-atom doping

Jialin Tang,[1,7] Qisheng Zeng,[1,7] Qiu Jiang,[1,2] Haoyuan Wang,[3] Sunpei Hu,[3] Yuan Ji,[1] Hongliang Zeng,[1] Chunxiao Liu,[1] Hong-Jie Peng,[2,4] Xu Li,[1] Tingting Zheng,[1] Chih-Wen Pao,[5,*] Xinyan Liu,[4,6,*] and Chuan Xia[1,2,8,*]

[1]School of Materials and Energy, University of Electronic Science and Technology of China, Chengdu, Sichuan 611731, P.R. China
[2]Yangtze Delta Region Institute (Huzhou), University of Electronic Science and Technology of China, Huzhou, Zhejiang 313001, P.R. China
[3]University of Science and Technology of China, Hefei National Research Center for Physical Sciences at the Microscale, Anhui 230026, P.R. China
[4]Institute of Fundamental and Frontier Sciences, University of Electronic Science and Technology of China, Chengdu, Sichuan 611731, P.R. China
[5]National Synchrotron Radiation Research Center, Science-Based Industrial Park, Hsinchu 30076, Taiwan
[6]Key Laboratory of Quantum Physics and Photonic Quantum Information, Ministry of Education, University of Electronic Science and Technology of China, Chengdu 611731, P.R. China
[7]These authors contributed equally
[8]Lead contact
*Correspondence: pao.cw@nsrrc.org.tw (C.-W.P.), xinyanl@uestc.edu.cn (X.L.), chuan.xia@uestc.edu.cn (C.X.)
https://doi.org/10.1016/j.checat.2025.101441

THE BIGGER PICTURE Ruthenium dioxide (RuO_2) has the potential to replace Ir-based catalysts for the oxygen evolution reaction (OER) in proton exchange membrane water electrolyzers (PEMWEs). However, achieving an optimal balance between catalytic activity and acid stability at high anodic potentials remains a critical challenge. Here, we present a palladium (Pd) and cobalt (Co) co-doping strategy to increase the activity and stability of rutile RuO_2 in the acidic OER. Consequently, the PdCo-RuO_2 catalyst exhibited a low overpotential of 190 mV at a current density of 10 mA cm^{-2} and maintained its activity for over 200 h at a large current density of 100 mA cm^{-2}, significantly outperforming pristine RuO_2. *In situ* measurements and density functional theory calculations revealed that Co doping favorably improves the intrinsic catalytic activity by weakening the overly strong Ru-O* interaction and reducing the energy barrier (ΔG) for the rate-determining OOH* deprotonation step, whereas Pd doping significantly enhances the acid stability of Ru active centers against over-oxidation and dissolution. When utilized as the anode electrocatalyst in a PEM electrolyzer, PdCo-RuO_2 achieves a low cell voltage of 1.6 V at a current density of 1 A cm^{-2} and maintains stable operation for over 350 h at 100 mA cm^{-2}. This work paves the way for designing more efficient and long-lasting OER electrocatalysts for industrial applications.

SUMMARY

Proton exchange membrane (PEM) water splitting is a cutting-edge technology that can produce clean and renewable hydrogen fuel. However, sluggish oxygen evolution reaction (OER) kinetics remain a challenge for the trade-off between catalytic activity and stability in acidic media. Currently, ruthenium dioxide (RuO_2) materials show great potential for the OER, which still suffers from a major drawback of low durability due to the severe dissolution of metal atoms in acidic electrolytes. Herein, we report a RuO_2 nanoparticle material modified with atomic Co and Pd to enhance OER stability while boosting catalytic activity in acidic environments. We demonstrate that Co atoms facilitate OOH* deprotonation, thereby lowering the OER energy barrier, while Pd atoms stabilize the Ru sites by effectively suppressing their over-oxidation and dissolution during the acidic OER.

INTRODUCTION

Proton exchange membrane water electrolysis (PEMWE) has emerged as a highly promising technology for green hydrogen production.[1,2] However, the development of highly efficient oxygen evolution reaction (OER) electrocatalysts is significantly challenging because of the sluggish kinetics of the anodic OER ($2H_2O \leftrightarrow O_2 + 4H^+ + 4e^-$) and the strongly acidic environment

Please cite this article in press as: Tang et al., Stabilization of highly active Ru sites toward acidic water oxidation by dual-atom doping, Chem Catalysis (2025), https://doi.org/10.1016/j.checat.2025.101441

within PEM devices.[3] To date, iridium (Ir)-based materials are considered the only qualified anode catalysts for PEMWE due to their excellent activity and stability.[4,5] However, the widespread adoption of Ir-based PEMWE has been largely constrained by the limited availability of Ir and its prohibitive cost (over \$60,000 kg^{-1}).[6,7] In contrast, ruthenium oxide (RuO_2)-based materials, which have high intrinsic activity and significantly lower cost (approximately \$9,500 kg^{-1}),[6] stand out as the most promising alternatives to Ir oxides for large-scale PEMWE.[8] Despite these advantages, RuO_2-based materials suffer from poor stability under strongly acidic conditions, primarily resulting from the irreversible oxidation of RuO_2 to soluble high-valence $Ru^{x>4}$ derivatives (e.g., RuO_4) at high potential (>1.4 V), leading to structural collapse and surface Ru leaching.[9,10] Therefore, the rational design of highly stable Ru-based OER electrocatalysts is indispensable for the practical implementation of PEMWE.

Typically, changes in the oxidation state of Ru sites within RuO_2-based OER electrocatalysts are closely associated with the kinetically favorable lattice oxygen mechanism (LOM) pathway.[11–13] Unlike the conventional adsorption evolution mechanism (AEM), the LOM reaction pathway involves the consumption of lattice oxygen to facilitate O–O coupling and O_2 generation.[14–16] This process is often accompanied by the formation of oxygen vacancies (O_{vac}),[17] which leave the Ru atoms adjacent to these vacancies highly exposed to the electrolyte. This process renders them highly susceptible to excessive oxidation and transient dissolution, ultimately leading to catalyst degradation.[9]

To stabilize Ru sites, the fundamental strategy involves modulating the electronic structure and suppressing the LOM pathway in the OER.[11,18–22] For example, research by Sargent et al. demonstrated that the involvement of lattice oxygen in the OER can be mitigated by engineering local Ru-O-Ir interactions, which significantly improved OER stability.[11] Similarly, Lee et al. proposed a Ru/MnO_2 catalyst that follows a unique oxide path mechanism (OPM). This pathway enables O–O radical coupling without generating O_{vac} and the participation of lattice oxygen, thereby preventing the Ru species from detaching from the catalyst surface.[14] Nevertheless, such a design principle involves complex mechanisms and has stringent requirements for the precise regulation of the metal active sites, making it difficult to fabricate homogeneous OPM-type OER electrocatalysts.[14,23,24]

To date, owing to the well-established relationship between OER stability and the electronic structure of Ru, enormous efforts have been made to reduce the average valence state of Ru as a pertinent descriptor of improved OER stability.[10,25–28] Among the various strategies proposed, the introduction of electron-donor elements (Li,[29] Sr,[30] Re,[31] W,[32] Zn,[33] etc.) has been shown to be effective in preventing the over-oxidation and dissolution of Ru sites, thereby enhancing OER stability. However, a significant drawback of these approaches is that the intrinsic catalytic activity may be compromised. The lower-valence Ru species, which are associated with weakened Ru-O covalency, tend to bind oxygen too weakly, leading to an increased operating potential for the catalyst.[10,18] Therefore, it is imperative to strike a balance between high catalytic activity and durability by stabilizing Ru active sites while concurrently improving the OER kinetics of Ru-based catalysts in acidic electrolytes.

In this study, we proposed a dual-modulation strategy that involves the incorporation of Pd and Co into the RuO_2 lattice to modulate the electronic structure and optimize the adsorption of OER intermediates. As a result, the PdCo–RuO_2 catalyst exhibited an impressively low overpotential of 190 mV at 10 mA cm^{-2} and demonstrated remarkable stability, maintaining performance for over 200 h at a high current density of 100 mA cm^{-2}. This represents an increase in stability of more than an order of magnitude compared with that of pristine RuO_2 catalysts. Through a combination of detailed experimental measurements and density functional theory (DFT) calculations, we revealed that the dual modulation of Co and Pd enables a hierarchical coupling effect that adjusts the electronic structure of Ru sites and optimizes the binding energy of oxo-intermediates, significantly enhancing both the OER activity and stability in acidic electrolytes. Mechanistic analysis attributes the exceptional electrocatalytic performance primarily to Co incorporation, which weakens the overly strong Ru–O* interaction and effectively reduces the energy barrier (ΔG) for the rate-determining OOH* deprotonation step, thereby enhancing the kinetic rate of the OER. Concurrently, the remarkable structural durability of PdCo–RuO_2 originates from the preferential oxidation of Pd^{2+}, which stabilizes Ru active centers through electron donating, thus enhancing resistance against oxidative degradation during prolonged electrocatalytic operation. When employed in a PEM electrolyzer, the PdCo–RuO_2||Pt/C assembly operates at a low cell voltage of 1.6 V at a current density of 1 A cm^{-2} and maintains stable performance for over 350 h at 100 mA cm^{-2}, demonstrating its potential for long-term, efficient energy conversion.

RESULTS AND DISCUSSION

Synthesis and characterization of the catalysts

PdCo–RuO_2 was prepared via a low-temperature molten salt method. The process began with a mixed molten salt solution of $NaNO_3$/KNO_3, in which the Ru^{3+} and Pd^{2+}/Co^{2+}precursors were dissolved. The controlled addition of these precursors allowed for the precise incorporation of Pd and Co into the RuO_2 lattice. The detailed synthesis procedure is provided in the methods section. The mass fractions of Pd and Co were examined using inductively coupled plasma-optical emission spectroscopy (ICP-OES) (Table S1), accounting for 0.9 and 0.38 wt %, respectively. The structure of PdCo-RuO_2 was identified by high-resolution X-ray diffraction (XRD) and high-angle annular dark-field scanning transmission electron microscopy (HAADF-STEM). As displayed in Figures 1A and S1, the XRD results show distinct diffraction peaks of (110), (101), (200), and (211) facets that can be indexed to rutile RuO_2 (ICSD: 43-1027),[18] suggesting that the incorporation of small amounts of Pd and Co has a minimal impact on the overall crystal structure. Additionally, Rietveld refinement analysis of the XRD data suggested that Pd and Co atoms are incorporated into the RuO_2 lattice through substitutional doping (Figure S2; Table S2), revealing a typical solid solution structure as described by Vegard's law.[22] HAADF-STEM images revealed that the PdCo–RuO_2 catalyst consists of small nanoparticles with an average diameter of around 3–5 nm (Figure S3). Notably, these nanoparticles exhibit a polycrystalline structure with well-defined lattice fringes of 0.32 and

Please cite this article in press as: Tang et al., Stabilization of highly active Ru sites toward acidic water oxidation by dual-atom doping, Chem Catalysis (2025), https://doi.org/10.1016/j.checat.2025.101441

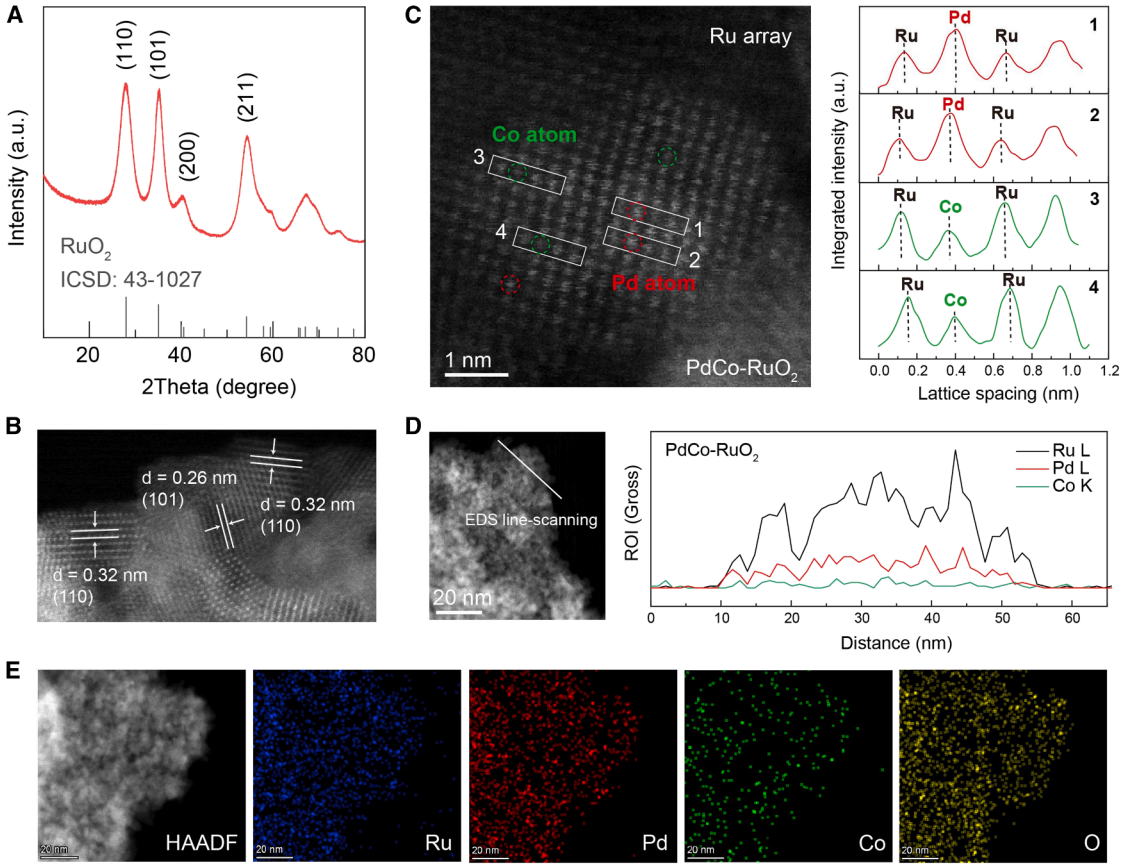

Figure 1. Atomic-scale structural characterization of PdCo–RuO_2

(A) XRD pattern of PdCo–RuO_2.

(B) HAADF-STEM image of PdCo–RuO_2.

(C) Local magnification of the HAADF-STEM image and identification of the incorporated Pd and Co from the corresponding atomic line profile. Red: Pd atom. Green: Co atom.

(D) EDS line scanning.

(E) TEM element mapping.

0.26 nm (Figure 1B), corresponding to the (110) and (101) planes of rutile-phase RuO_2,[33,34] respectively. Undoped RuO_2 as a control sample shows typically identical lattice spacings of the (110) and (101) planes to those of the PdCo–RuO_2, suggesting a negligible lattice distortion upon micro-doping of Pd and Co (Figure S4). To visually identify the presence of Pd and Co within the structure, a magnified HAADF-STEM image displaying a highly ordered arrangement of metal atoms was extracted (Figure 1C). Owing to the characteristics of lighter elements exhibiting lower imaging contrast, isolated Pd atoms and Co atoms were observed within the lattice, indicating a high dispersion of Pd and Co within the RuO_2 structure. The spatial distributions of Ru, Pd, and Co without element segregation were further confirmed by energy-dispersive spectrometry (EDS) analysis (Figures 1D and S5) and TEM elemental mapping (Figure 1E), revealing the heterogeneous composition of the sample surface.

Electrochemical OER performance in acidic media

Electrochemical measurements were subsequently performed to assess the OER performance of the PdCo–RuO_2 catalyst in a 0.5 M H_2SO_4 electrolyte. For comparison, control samples were also evaluated under identical conditions. As demonstrated in Figure 2A, the PdCo–RuO_2 catalyst achieved a current density of 10 mA cm^{-2} at a remarkably low overpotential (η_{10}) of 190 mV, surpassing the OER activities of the as-synthesized RuO_2 (200 mV), Pd–RuO_2 (193 mV), and commercial RuO_2 (270 mV) counterparts (Figure S6). Notably, Co–RuO_2 exhibited superior catalytic performance (η_{10} = 190 mV) compared to PdCo-RuO_2, highlighting the dominant role of Co doping in enhancing OER activity. Kinetic analysis derived from Tafel plots (Figure 2B) revealed favorable charge transfer characteristics for Co-containing catalysts, with Tafel slopes of 46.3 mV dec^{-1} for Co–RuO_2, 53.6 mV dec^{-1} for PdCo–RuO_2, 61.3 mV dec^{-1} for Pd–RuO_2, and 59.6 mV dec^{-1} for pristine RuO_2. This trend confirms that Co incorporation significantly accelerates the OER kinetics. Complementary electrochemical impedance spectroscopy (EIS) measurements at 1.45 V versus reversible hydrogen electrode (RHE) (Figure S7) showed substantially reduced charge transfer resistances for both PdCo–RuO_2 and Co–RuO_2 compared to other samples, further corroborating the

Please cite this article in press as: Tang et al., Stabilization of highly active Ru sites toward acidic water oxidation by dual-atom doping, Chem Catalysis (2025), https://doi.org/10.1016/j.checat.2025.101441

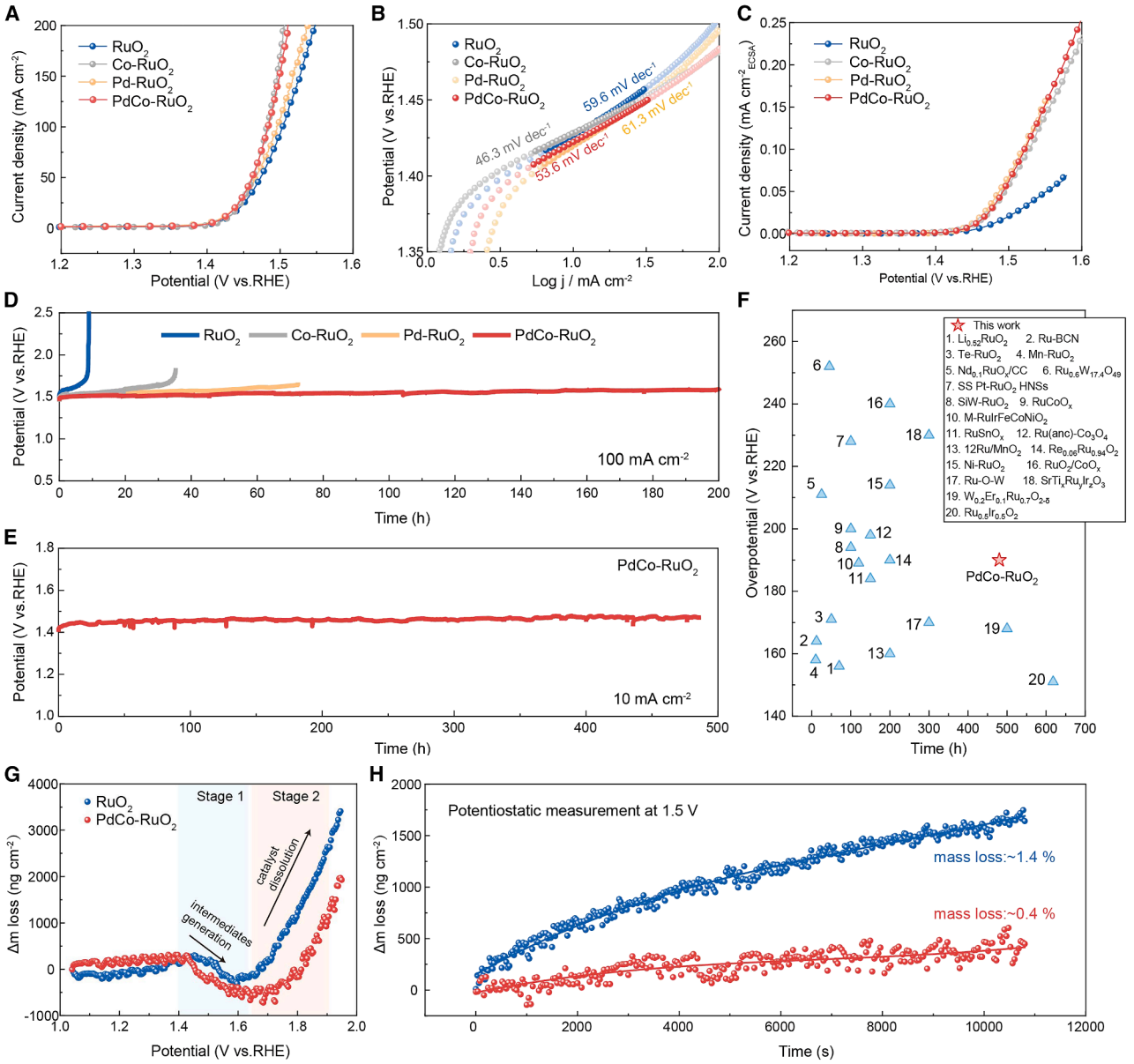

Figure 2. Electrochemical performance of the as-prepared catalysts

(A) LSV results of the as-prepared samples. Carbon paper was used as working electrode support.

(B) Derived Tafel plots of the as-prepared samples.

(C) ECSA-normalized LSV curves. The glassy carbon was used as working electrode support.

(D) CP tests of the as-prepared samples at a fixed current density of 100 mA cm^{-2}.

(E) CP tests of PdCo–RuO_2 at a fixed current density of 10 mA cm^{-2}.

(F) Comparison of the overpotentials and catalytic stability at 10 mA cm^{-2} for recently reported ruthenium-based oxide catalysts in the acidic OER. Catalyst references can be found in Table S3.

(G) Results of an EQCM LSV measurements (2 mV s^{-1}) of the as-synthesized RuO_2 and PdCo–RuO_2.

(H) Results of an EQCM potentiostatic measurement of the as-prepared RuO_2 and PdCo–RuO_2 at 1.5 V vs. RHE.

enhanced charge transfer efficiency induced by Co doping. Surface characterization through cyclic voltammetry in the non-faradaic region (Figures S8 and S9) yielded double-layer capacitance (C_{dl}) values of 8.3 mF cm^{-2} for PdCo–RuO_2 and 38.5 mF cm^{-2} for pristine RuO_2, corresponding to electrochemical active surface areas (ECSAs) of 215.4 and 999 cm^2, respectively. The reduced ECSA of PdCo-RuO_2 suggests that surface-distributed dopant atoms may partially block Ru active sites. However, when normalized by ECSA (Figure 2C), PdCo–RuO_2 demonstrated significantly higher intrinsic activity with lower overpotential and

Please cite this article in press as: Tang et al., Stabilization of highly active Ru sites toward acidic water oxidation by dual-atom doping, Chem Catalysis (2025), https://doi.org/10.1016/j.checat.2025.101441

greater current density than pure RuO_2, indicating that atomic-level modifications through doping effectively optimize the catalytic properties of surface Ru sites. These comprehensive analyses collectively demonstrate that while PdCo–RuO_2 possesses fewer exposed active sites, the synergistic effects of Co and Pd doping remarkably enhance the intrinsic activity of remaining Ru sites through electronic structure modulation and improved charge transfer kinetics, ultimately leading to superior OER performance.

To further assess catalyst stability, an accelerated degradation test was performed at a fixed current density of 100 mA cm^{-2} (Figure 2D). It revealed that the synthesized RuO_2 catalyst degraded rapidly within 20 h, which is consistent with previous reports.[4,35,36] In comparison, the synthesized Co–RuO_2 and Pd-RuO_2 samples maintained better structural integrity, with a slower activity decay rate than RuO_2. Remarkably, PdCo–RuO_2 showed a significant improvement in catalytic stability, operating stably for over 200 h, far exceeding the performance of Co–RuO_2 and Pd–RuO_2 samples. This finding suggests that the synergistic effects of Co and Pd doping remarkably improve the catalytic stability compared to the single-doped counterparts. We further conducted a continuous chronopotentiometry (CP) test of the PdCo–RuO_2 catalyst at a current density of 10 mA cm^{-2} (Figure 2E). Surprisingly, PdCo–RuO_2 demonstrated exceptional long-term durability for more than 480 h, surpassing most of the reported Ru-based oxide catalysts in acidic electrolytes (Figure 2F; Table S3). These results collectively suggest that PdCo–RuO_2 holds substantial promise for acidic water oxidation, offering both exceptional activity and prolonged stability.

The dissolution of the catalyst under operational conditions is considered the primary cause of catalyst deactivation, which ultimately leads to the degradation of OER performance. To better understand the dissolution behavior of the catalyst, an electrochemical quartz crystal microbalance (EQCM) was applied to detect the mass change of the catalysts precisely during the electrochemical reactions (see methods for more details). The change in mass was monitored as a function of the resonant frequency (Hz) via the Sauerbrey equation.[37–39] First, the EQCM test was performed under a linear sweep voltammetry (LSV) scan from 1.05 to 1.95 V vs. RHE for both the PdCo–RuO_2 and RuO_2 catalysts (Figures 2G and S10). As the potential increased from 1.40 to 1.65 V (stage one), a negative mass loss was observed, indicating that more oxo-intermediates were generated on the catalyst surface during the OER. Within this potential range, the mass increase of the PdCo–RuO_2 catalyst is greater than that of RuO_2, revealing a higher production rate of the oxo-intermediates during the OER. When the potential exceeds 1.65 V (stage two), rapid positive mass loss is observed, which is caused primarily by extensive catalyst leaching from the catalyst surface. To better evaluate the catalyst dissolution behavior, a potentiostatic measurement was performed at a moderate potential of ~1.5 V, which enables a dynamic equilibrium between oxo-intermediate generation and catalyst leaching (Figures 2H and S11). Over a 3-h period, the RuO_2 catalyst exhibited a substantial mass loss of approximately ~1.4%, which was approximately 3.5 times greater than the mass loss of ~0.4% observed for PdCo–RuO_2. These results clearly demonstrate that catalyst leaching into the electrolyte is significantly lower in PdCo–RuO_2 than in RuO_2.

Origin of the improved OER performance of PdCo-RuO_2

The dissolution of high-valence Ru is considered the cause of the deactivation of the catalyst during the OER process. To elucidate the evolution of the Ru valence state during the OER, *in situ* X-ray absorption near-edge structure (XANES) spectroscopy was performed on the as-prepared samples at the Ru *K*-edge at different potentials. As shown in Figures 3A and S12, with increasing applied potential, the Ru sites in both the PdCo–RuO_2 and RuO_2 catalysts were oxidized to higher valence states (Ru^x, $x > +4$). Specifically, the absorption threshold positions of Ru in PdCo–RuO_2 are lower than those of RuO_2 at all applied potentials. This suggests that the Ru sites in PdCo–RuO_2 demonstrate a slightly lower valence state at high potentials, which may contribute to the catalyst's enhanced stability during the acidic OER. These findings are further supported by the X-ray photoelectron spectroscopy (XPS) results of the PdCo–RuO_2 and RuO_2 catalysts (Figure S13).[26,40] The changes in the coordination environment of Ru–O for the as-prepared samples are revealed by the extended X-ray absorption fine structure (EXAFS) (Figure 3B). The first coordination peak, centered at approximately 1.5Å, corresponds to the Ru–O shell.[41] EXAFS fitting was performed to quantitatively assess the changes in the Ru–O bond length and coordination number (CN) under working conditions, and the detailed curves and parameters are provided in Figures S14 and S15 and Table S4. As the applied potential is increased, the pristine RuO_2 shows a shortened Ru–O bond length from 1.97 to 1.95 Å in the OER region, while the PdCo–RuO_2 retained a constant Ru–O bond length of 1.97 Å across all tested potentials (Figure 3C), indicating its structural stability. This stable Ru-O configuration also indicates a weakened Ru–O covalency under operating conditions, which likely shifts the O 2*p* orbital below the Fermi level, thereby optimizing intermediate adsorption and suppressing the involvement of lattice oxygen in the OER process.[4,18,42,43] The CN of pristine RuO_2 decreases markedly from 3.9 to 3.6 under identical conditions, indicative of the formation of structurally vulnerable unsaturated RuO_x species, while the CN of PdCo–RuO_2 remains invariant at 3.2 across increasing potentials (Figure 3D), suggesting the lattice oxygen atoms are stabilized in the matrix. Comparative TEM analysis revealed distinct structural differences between post-OER PdCo–RuO_2 and pristine RuO_2 (Figures S16 and S17). Specifically, pristine RuO_2 undergoes significant surface corrosion, whereas the PdCo–RuO_2 catalyst retains well-resolved lattice fringes indexed to the (101) and (110) planes of rutile-phase RuO_2 under identical OER conditions. Collectively, these results underscore the critical role of Pd/Co dual-atom doping in preserving both the local coordination geometry and global structural integrity under OER-working conditions.

The X-ray absorption spectroscopy (XAS) technique was employed to provide mechanistic insights into the electronic and structural contributions of cobalt. Detailed analysis of the Co *K*-edge EXAFS spectra reveals the predominant presence of Co–O scattering paths with the complete absence of Co–Co signatures (Figure S18), confirming the atomic-level dispersion of Co within the RuO_2 lattice. The shortened Co–O bond length (1.45 vs. 1.51 Å in standard CoOOH) revealed by wavelet transform analysis in *R* space enhanced covalent bonding through Co–O–Ru linkages[44] (Figure S18). EXAFS results show a

Please cite this article in press as: Tang et al., Stabilization of highly active Ru sites toward acidic water oxidation by dual-atom doping, Chem Catalysis (2025), https://doi.org/10.1016/j.checat.2025.101441

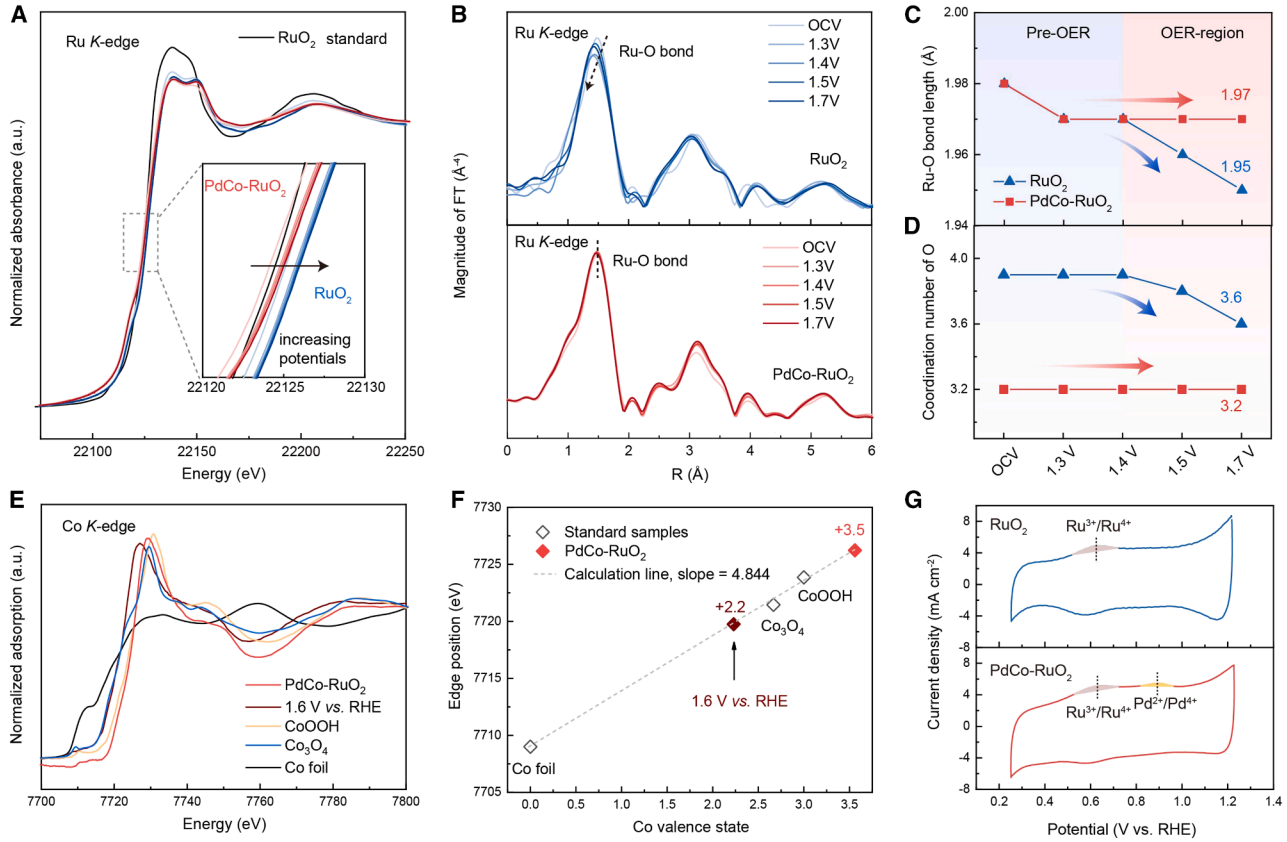

Figure 3. Analysis of the electronic structure of the as-prepared catalysts

(A) *Operando* XANES results at the Ru *K*-edge of synthesized RuO_2 and PdCo–RuO_2. Rutile-phase RuO_2 was used as the benchmark.

(B) *Operando* EXAFS results at the Ru *K*-edge of the synthesized RuO_2 and PdCo–RuO_2. All the EXAFS spectra are displayed without phase correction.

(C) Fitting results of the Ru–O bond length of the synthesized RuO_2 and PdCo–RuO_2 as a function of the applied potential.

(D) Fitting results of the Ru–O coordination number of the synthesized RuO_2 and PdCo–RuO_2 as a function of the applied potential.

(E) XANES results at the Co *K*-edge of the pre–PdCo–RuO_2 and potential-applied conditions (1.6 V vs. RHE).

(F) Changes in the Co valence state of the pre–PdCo–RuO_2 and potential-applied conditions. Linearity was obtained for the Co foil, Co_3O_4, and CoOOH standard samples.

(G) Cyclic voltammetry curves of synthesized RuO_2 and PdCo–RuO_2.

dominant peak at approximately 3.18 Å in the second coordination sphere, corresponding to Co–O–Ru coordination. This distance closely aligns with the Ru–O–Ru coordination length (3.1 Å) in crystalline RuO_2, providing strong evidence for the substitutional incorporation of Co atoms into the RuO_2 lattice. This atomic dispersion of Co within the oxide matrix induces structural reinforcement via a strong electron coupling effect,[43] effectively stabilizing Co atoms. The XANES results (Figures 3E and 3F) show that pristine PdCo-RuO_2 has a Co *K*-edge absorption energy corresponding to an average oxidation state of +3.5, indicating the coexistence of Co^{3+} and Co^{4+} species. This mixed high-valence Co^{3+}/Co^{4+} generates strongly electronegative centers that withdraw electron density from adjacent Ru sites, creating electron-deficient Ru active sites. Under operational conditions at 1.6 V vs. RHE, the Co centers undergo reduction to lower valence states of +2.2 (Co^{2+}/Co^{3+}) under OER conditions, acting as redox buffers to transiently stabilize reaction intermediates (e.g., OOH* ↔ O* transitions). This dynamic electronic tuning creates optimized adsorption sites for oxygenated intermediates via the Sabatier principle, weakening the overly strong Ru–O* interaction[44] and promoting the OER process.

Cyclic voltammetry was conducted to investigate the redox behavior of the metal sites (Figure 3G). The as-prepared samples displayed a redox peak at approximately 0.62 V, corresponding to the Ru^{3+}/Ru^{4+} redox transitions.[32,35] Notably, PdCo–RuO_2 exhibited a pronounced redox peak at approximately 0.90 V, corresponding to the Pd^{2+}/Pd^{4+} redox transition (Figure S19), suggesting that surface Pd sites are oxidized to higher valence states before the OER begins. This was further validated by Pd 3*d* XPS analysis of the post-catalysis PdCo–RuO_2 (Figure S20). We propose that the preferential oxidation of Pd^{2+} facilitates dynamic electron transfer from Pd to nearby Ru sites, mitigating their over-oxidation and dissolution during the OER, thereby enhancing the stability of the catalyst. Electron paramagnetic resonance (EPR) spectroscopy (Figure S21) detected a pronounced oxygen vacancy (O_{vac}) signal (g = 2.003) in PdCo–RuO_2, signifying a high concentration of defect sites. The observed enrichment of O_{vac} can be attributed to the

Please cite this article in press as: Tang et al., Stabilization of highly active Ru sites toward acidic water oxidation by dual-atom doping, Chem Catalysis (2025), https://doi.org/10.1016/j.checat.2025.101441

incorporation of low-valent Pd^{2+} dopants,[45,46] as evidenced by XPS analysis (Figure S22). These induced vacancies not only provide additional active sites for the OER but also stabilize the lattice against Jahn-Teller distortions.

OER mechanism analysis

To investigate the catalytic reaction mechanism effectively and the associated variations in the electronic structure of Ru, *in situ* attenuated total reflectance surface-enhanced infrared absorption spectroscopy (ATR-SEIRAS) measurements were performed on the RuO_2 and PdCo-RuO_2 materials under different applied potentials. As the potential increased to 1.7 V (Figures 4A and 4B), two distinctive peaks at approximately 1,212 and 1,000–1,100 cm^{-1} were observed for both samples, corresponding to the vibrational modes of the OOH* and OO* intermediates, respectively. The OO*/OOH* ratio serves as a critical parameter for quantifying the relative contributions of AEM (characterized by OOH* intermediates) and LOM (dominated by OO* species formation).[4,47] As shown in Figure 4C, pristine RuO_2 has significantly higher OO*/OOH* ratios (~16.7%) than PdCo–RuO_2 (~7.2%), indicating stronger LOM participation in RuO_2 and a preferential AEM pathway in the doped catalyst. These findings strongly suggest that the synergistic interplay of Co and Pd dopants triggers a charge density redistribution within the RuO_2 lattice. This electronic modulation suppresses the participation of lattice oxygen in PdCo–RuO_2, thereby lowering the production of OO* intermediates.

DFT calculations were further employed to investigate the effects of Co and Pd doping on the catalytic properties. The doping effect was considered separately rather than jointly because the low doping amount of Co and Pd corresponds to a low probability of both dopants neighboring. The slab model exposing the rutile-phase RuO_2 (110) was constructed for its lowest surface energy and adopted as the baseline model for generating slabs with an oxygen vacancy (O_{vac}; denoted by the suffix of -O_{vac}) and with a Ru atom substituted by a dopant atom (denoted as Co–RuO_2 and Pd–RuO_2). As shown in Figure 4D, the lattice oxygen atom bridging two Ru atoms tends to be preferably removed, leaving an O_{vac} on the surface. The O_{vac} formation energy (ΔE_{Ovac}) was obtained by computing the energetic differences of the oxygen atom at the bridge site and in a water molecule, which were −0.03, −0.92, and −1.26 eV for RuO_2, Co–RuO_2, and Pd–RuO_2, respectively. Thus, surface O_{vac} formation can be largely facilitated through Co/Pd doping, especially through the introduction of Pd, rationalizing the experimental EPR results. By considering a classical adsorbate evolution mechanism, as corroborated by ATR-SEIRAS and previous investigations,[31] the catalytic superiorities of such O_{vac}-rich surfaces are further illustrated in Figure 4E. The universal scaling between the binding strengths of the OH* and OOH* intermediates ($\Delta G_{OOH^*} = \Delta G_{OH^*} + 3.0$ eV, considering the different solvation effects on stabilizing OH* and OOH*)[48] was leveraged to obtain a two-dimensional OER activity volcano plot, in which the theoretical overpotential η can be expressed as a function of the OH* binding energy (ΔG_{OH^*}) and the difference in adsorption strengths between O* and OH* ($\Delta G_{O^*} - \Delta G_{OH^*}$) (see the supplemental information for details). The surfaces that contain O_{vac} are shown to possess more ideal binding strengths and are located closer to the volcano peak featuring moderate oxygen reactivity. The corresponding free energy diagrams are additionally compared at a potential of 1.23 V vs. RHE (Figure 4F). The optimized geometries of OH*, O*, and OOH* adsorbed on these slabs, as well as the corresponding surfaces without adsorbates, are depicted in Figure S23. All surfaces except Co–RuO_2–O_{vac} exhibit a potential-determining step (PDS), in which water nucleophilically attacks the coordinatively unsaturated oxygen (O_{CUS}) to yield OOH*, among which RuO_2–O_{vac} has the lowest free energy penalty of 0.38 eV (Figure S24). The Co–RuO_2–O_{vac} surface, however, experiences a shift of the PDS to the last step of OOH* deprotonation to liberate O_2, which results in an even lower free energy penalty of 0.34 eV. To rationalize such enhancement, the projected density of states (PDOS) analysis of the O–2*p* orbitals of the O_{CUS} atom was plotted. As shown in Figure 4G, O_{vac} formation and Co/Pd doping populate more states at higher energies. The *p*-band center $\bar{\varepsilon}_{O\_2p}$ was computed for further comparison (Figure 4H). The Co-RuO_2–O_{vac} surface has the highest $\bar{\varepsilon}_{O\_2p}$ of −2.69 eV, whereas the O_{vac}- and dopant-free baseline surfaces have the lowest $\bar{\varepsilon}_{O\_2p}$ of −2.92 eV. This finding aligns well with previous theories that $\bar{\varepsilon}_{O\_2p}$ is positively correlated with oxygen reactivity and that a higher $\bar{\varepsilon}_{O\_2p}$ of O_{CUS} makes it easier for water to undergo nucleophilic attack.[49] Note that Pd doping is not as superior as Co doping in regulating the OER energetics to the optimum value. However, the introduction of Pd largely stabilizes the more active O_{vac}-containing structures. Along with the Co doping that further boosts the OER performance through the modulation of the local electronic structure of O_{vac}-rich RuO_2 surfaces, the great catalytic potential of PdCo–RuO_2 for the acidic OER is thereby substantiated.

Performance of PEMWE devices

Finally, we assembled a PEM electrolyzer (Figure 5A) to evaluate the overall water-splitting performance (see the supplemental information for details). The fabricated membrane electrode assembly (MEA) was characterized using SEM in both cross-sectional and planar views (Figures 5B and S25). The MEA consisted of an anode PdCo–RuO_2 (2 mg cm^{-2}) catalyst, a cathode Pt/C (0.8 mg cm^{-2}) catalyst, and a PEM (Nafion 117). The single PEM cell was tested at an operating temperature of 80°C using carbon paper and Ti felt as the porous transport layers (PTLs). The current-voltage (*J*–*V*) curves (without *iR*-compensation) (Figure 5C) revealed that the PdCo–RuO_2||Pt/C assembly required cell voltages of only 1.6 and 1.688 V to achieve current densities of 1 and 2 A cm^{-2}, respectively. These values are significantly lower than those required by the reference commercial RuO_2||Pt/C and even Co–RuO_2||Pt/C assemblies under elevated current density exceeding 500 mA cm^{-2} (Figure S26), highlighting its exceptional electrocatalytic activity. In comparison with other newly reported Ru- or Ir-based oxides applied in the PEM anode, PdCo–RuO_2 exhibits comparably small cell voltages under industrial current densities of 1 and 2 A cm^{-2} (Figure 5D; Table S5). We further conducted an economic analysis to compare the performance of the PEM devices (see the supplemental information for details). The PEM energy efficiency when PdCo-RuO_2 is used as the anode reaches 72.86% at 2 A cm^{-2}, with a corresponding energy consumption of 45.24 kWh kg^{-1} (Table S6). Specifically, the estimated cost per kilogram

Please cite this article in press as: Tang et al., Stabilization of highly active Ru sites toward acidic water oxidation by dual-atom doping, Chem Catalysis (2025), https://doi.org/10.1016/j.checat.2025.101441

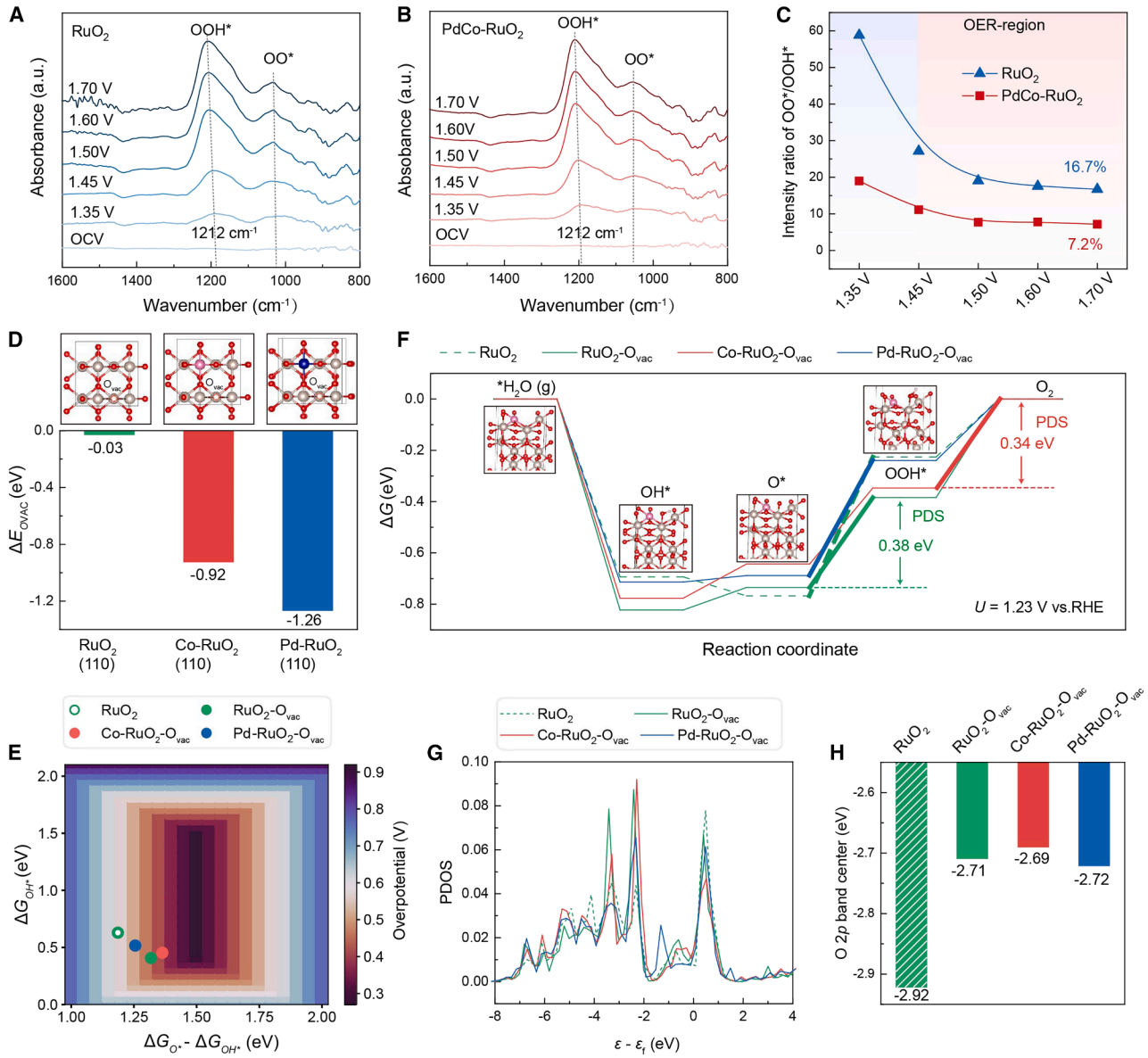

Figure 4. Mechanistic analysis of PdCo–RuO_2 toward the acidic OER

(A and B) *In situ* ATR-SEIRAS analysis of (A) RuO_2 and (B) PdCo–RuO_2.

(C) Normalized intensity of OOH*/OO* as a function of the applied potential obtained from the ATR-SEIRAS results.

(D) Formation energy of the oxygen vacancy (O_{vac}) in RuO_2 (110), Co–RuO_2 (110), and Pd–RuO_2 (110).

(E) Theoretical two-dimensional overpotential map as a function of ΔG_{OH^*} and $\Delta G_{O^*} - \Delta G_{OH^*}$.

(F) Free energy diagrams of the OER on RuO_2, RuO_2–O_{vac}, Co–RuO_2–O_{vac}, and Pd–RuO_2–O_{vac} at U = 1.23 V vs. RHE. The bold lines indicate the potential-determining steps (PDSs). Using Co–RuO_2–O_{vac} as an example, the surface without adsorbates and optimized geometries of OH*, O*, and OOH* adsorbed on the slab are depicted.

(G) PDOS of the O 2*p* orbitals of O*-adsorbed RuO_2, RuO_2–O_{vac}, Co–RuO_2–O_{vac}, and Pd–RuO_2–O_{vac}.

(H) O 2*p* band center obtained from the PDOS.

of H_2 produced using our PEM device is approximately \$0.9, which is significantly lower than the Department of Energy (DOE) target of \$2 per kilogram by 2026. We further evaluated the stability of the PEM device utilizing the PdCo–RuO_2 catalyst as an anode at 80°C (Figure 5E). When a constant density of 100 mA cm^{-2} was applied, the cell voltage of the PdCo–RuO_2|| Pt/C assembly did not significantly increase for 350 h. Even when operating at a higher current density of 200 mA cm^{-2}, it achieves 160 h of stability (<10% decay), representing an 8-fold improvement over that of pristine RuO_2 (<20 h). These results confirm the superior OER stability of the PdCo–RuO_2 catalyst and highlight its potential suitability for use in PEM devices.

Please cite this article in press as: Tang et al., Stabilization of highly active Ru sites toward acidic water oxidation by dual-atom doping, Chem Catalysis (2025), https://doi.org/10.1016/j.checat.2025.101441

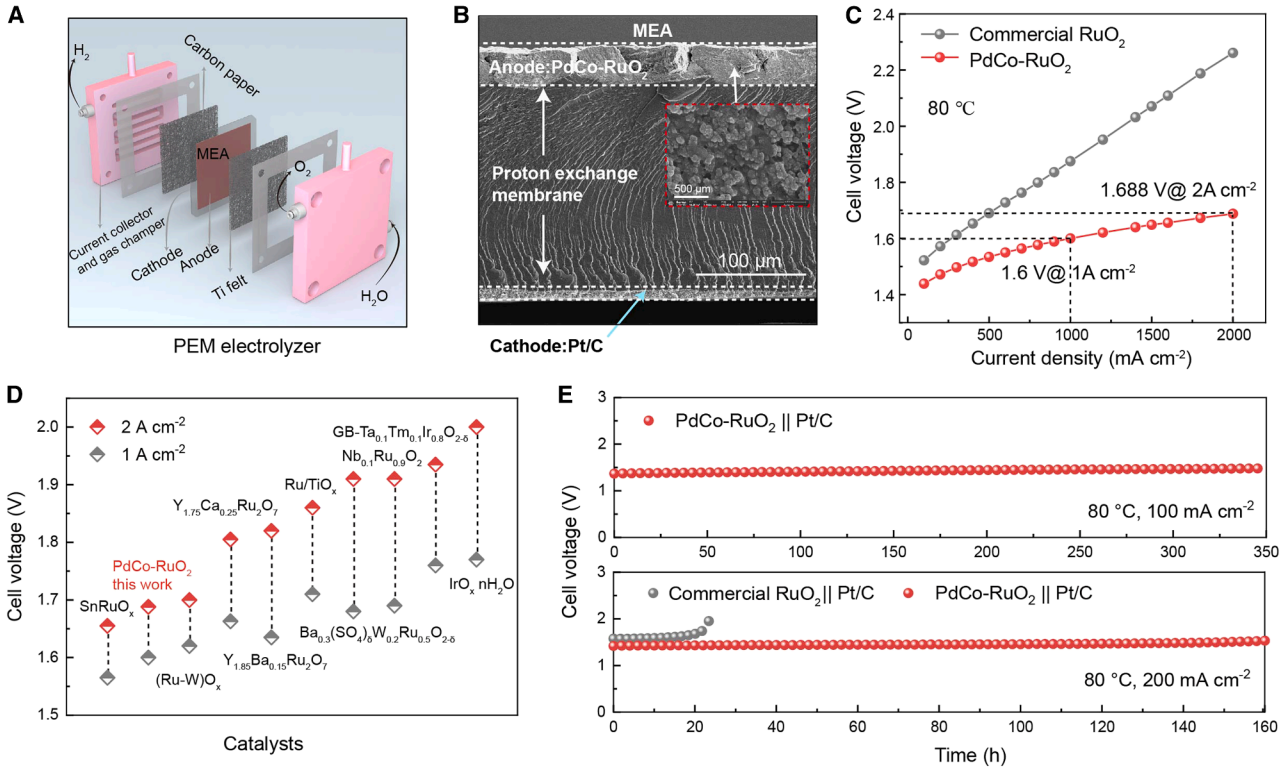

Figure 5. PEM performance evaluation

(A) Schematic diagram of the PEM electrolyzer.

(B) SEM side view of the fabricated MEA.

(C) *J-V* curves of commercial RuO_2 and PdCo–RuO_2 at 80°C.

(D) Comparison of the cell voltages of PdCo–RuO_2 and other reported representative Ru/Ir-based oxide OER catalysts at 1 and 2 A cm^{-2}.

(E) Chronopotentiometry stability tests measured at fixed current densities of 100 mA cm^{-2} for PdCo–RuO_2 and 200 mA cm^{-2} for commercial RuO_2 and PdCo–RuO_2. Pure water was used as the electrolyte.

Conclusion

In summary, we reported a highly active and durable OER electrocatalyst in acid by incorporating Pd and Co into the RuO_2 lattice. The resulting PdCo–RuO_2 catalyst demonstrated an impressively low overpotential of only 190 mV at 10 mA cm^{-2} and exhibited excellent stability, maintaining its performance for over 200 h at a large current density of 100 mA cm^{-2}. *In situ* measurements and DFT calculations revealed that Co doping can effectively optimize the adsorption energy of oxygen-containing intermediates and reduce the energy barrier for OOH* deprotonation through Co–O–Ru interactions, leading to improved OER activity. Pd doping prevents excessive oxidation of Ru and stabilizes the Ru active sites via electron transfer, thereby increasing the OER stability in acidic electrolytes. This study highlights the critical role of Co and Pd co-doping in modulating the electronic structure of Ru active centers and achieving an optimal balance between catalytic activity and stability under acidic OER conditions. When applied in a PEM electrolyzer, the PdCo–RuO_2 catalyst achieved a low cell voltage of 1.6 V at a current density of 1 A cm^{-2} and operated stably for 350 h at 100 mA cm^{-2}. This work provides valuable insights into the degradation mechanisms of Ru-based catalysts and presents a promising strategy for designing high-performance, stable electrocatalysts for acidic OER applications.

METHODS

Details regarding the methods can be found in the supplemental information.

RESOURCE AVAILABILITY

Lead contact

Further information and requests for resources should be directed to and will be fulfilled by the lead contact, Chuan Xia (chuan.xia@uestc.edu.cn).

Materials availability

Materials generated in this study will be made available upon request, but we may require a payment and/or a completed material transfer agreement if there is potential for commercial application.

Data and code availability

The data generated during this study are available from the lead contact upon request.

ACKNOWLEDGMENTS

We acknowledge the National Key Research and Development Program of China (2024YFB4105700), the National Natural Science Foundation of China (52171201, 22322201, 22278067, 22305029, and 22405035), the Natural Science Foundation of Sichuan Province (2025NSFJQ0017, 2023NSFSC1075, and 2024NSFSC1104), the Huzhou Science and Technology Bureau (2022GZ45 and 2023GZ02) and a China Postdoctoral Science Foundation-funded project (2022M710601). We thank beamline BL11B of the Shanghai Synchrotron Radiation Facility, 44A of the Taiwan Photon Source (TPS) at the National Synchrotron Radiation Research Center, and PD of the Australia Synchrotron for providing the beamtime.

AUTHOR CONTRIBUTIONS

This work was conceptualized by C.X. and supervised by C.X. and C.-W.P. J.T. and Q.Z. prepared the catalysts and performed the catalytic tests. Y.J., H.W., S.H., H.Z., and C.L. performed the catalyst characterizations. X.L. and H.-J.P. performed the DFT calculations. J.T. wrote the paper with input from all authors. Q.J., X.L., and T.Z. modified the paper. All the authors discussed the results and commented on the manuscript.

DECLARATION OF INTERESTS

A China provisional patent application (2024107687155) based on the technology described in this work was filed at the University of Electronic Science and Technology of China.

SUPPLEMENTAL INFORMATION

Supplemental information can be found online at https://doi.org/10.1016/j.checat.2025.101441.

Received: January 14, 2025
Revised: February 20, 2025
Accepted: June 9, 2025

REFERENCES

1. Carmo, M., Fritz, D.L., Mergel, J., and Stolten, D. (2013). A comprehensive review on PEM water electrolysis. Int. J. Hydrogen Energy *38*, 4901–4934. https://doi.org/10.1016/j.ijhydene.2013.01.151.
2. Tao, H.B., Liu, H., Lao, K., Pan, Y., Tao, Y., Wen, L., and Zheng, N. (2024). The gap between academic research on proton exchange membrane water electrolysers and industrial demands. Nat. Nanotechnol. *19*, 1074–1076. https://doi.org/10.1038/s41565-024-01699-x.
3. Hao, S., Sheng, H., Liu, M., Huang, J., Zheng, G., Zhang, F., Liu, X., Su, Z., Hu, J., Qian, Y., et al. (2021). Torsion strained iridium oxide for efficient acidic water oxidation in proton exchange membrane electrolyzers. Nat. Nanotechnol. *16*, 1371–1377. https://doi.org/10.1038/s41565-021-00986-1.
4. Li, L., Zhang, G., Zhou, C., Lv, F., Tan, Y., Han, Y., Luo, H., Wang, D., Liu, Y., Shang, C., et al. (2024). Lanthanide-regulating Ru-O covalency optimizes acidic oxygen evolution electrocatalysis. Nat. Commun. *15*, 4974. https://doi.org/10.1038/s41467-024-49281-2.
5. Shi, Z., Li, J., Jiang, J., Wang, Y., Wang, X., Li, Y., Yang, L., Chu, Y., Bai, J., Yang, J., et al. (2022). Enhanced Acidic Water Oxidation by Dynamic Migration of Oxygen Species at the Ir/Nb_2O_{5-x} Catalyst/Support Interfaces. Angew. Chem. Int. Ed. *61*, e202212341. https://doi.org/10.1002/anie.202212341.
6. Zhou, L., Shao, Y., Yin, F., Li, J., Kang, F., and Lv, R. (2023). Stabilizing non-iridium active sites by non-stoichiometric oxide for acidic water oxidation at high current density. Nat. Commun. *14*, 7644. https://doi.org/10.1038/s41467-023-43466-x.
7. Zhai, W., Ma, Y., Chen, D., Ho, J.C., Dai, Z., and Qu, Y. (2022). Recent progress on the long-term stability of hydrogen evolution reaction electrocatalysts. InfoMat *4*, e12357. https://doi.org/10.1002/inf2.12357.
8. Wang, J., Yang, H., Li, F., Li, L., Wu, J., Liu, S., Cheng, T., Xu, Y., Shao, Q., and Huang, X. (2022). Single-site Pt-doped RuO_2 hollow nanospheres with interstitial C for high-performance acidic overall water splitting. Sci. Adv. *8*, eabl9271. https://doi.org/10.1126/sciadv.abl9271.
9. Xue, Y., Zhao, J., Huang, L., Lu, Y.-R., Malek, A., Gao, G., Zhuang, Z., Wang, D., Yavuz, C.T., and Lu, X. (2023). Stabilizing ruthenium dioxide with cation-anchored sulfate for durable oxygen evolution in proton-exchange membrane water electrolyzers. Nat. Commun. *14*, 8093. https://doi.org/10.1038/s41467-023-43977-7.
10. Shi, Z., Li, J., Wang, Y., Liu, S., Zhu, J., Yang, J., Wang, X., Ni, J., Jiang, Z., Zhang, L., et al. (2023). Customized reaction route for ruthenium oxide towards stabilized water oxidation in high-performance PEM electrolyzers. Nat. Commun. *14*, 843. https://doi.org/10.1038/s41467-023-36380-9.
11. Wen, Y., Chen, P., Wang, L., Li, S., Wang, Z., Abed, J., Mao, X., Min, Y., Dinh, C.T., Luna, P.D., et al. (2021). Stabilizing Highly Active Ru Sites by Suppressing Lattice Oxygen Participation in Acidic Water Oxidation. J. Am. Chem. Soc. *143*, 6482–6490. https://doi.org/10.1021/jacs.1c00384.
12. Yao, Y., Hu, S., Chen, W., Huang, Z.-Q., Wei, W., Yao, T., Liu, R., Zang, K., Wang, X., Wu, G., et al. (2019). Engineering the electronic structure of single atom Ru sites via compressive strain boosts acidic water oxidation electrocatalysis. Nat. Catal. *2*, 304–313. https://doi.org/10.1038/s41929-019-0246-2.
13. He, W., Tan, X., Guo, Y., Xiao, Y., Cui, H., and Wang, C. (2024). Grain-Boundary-Rich RuO_2 Porous Nanosheet for Efficient and Stable Acidic Water Oxidation. Angew. Chem. Int. Ed. *63*, e202405798. https://doi.org/10.1002/anie.202405798.
14. Lin, C., Li, J.-L., Li, X., Yang, S., Luo, W., Zhang, Y., Kim, S.-H., Kim, D.-H., Shinde, S.S., Li, Y.-F., et al. (2021). In-situ reconstructed Ru atom array on α-MnO_2 with enhanced performance for acidic water oxidation. Nat. Catal. *4*, 1012–1023. https://doi.org/10.1038/s41929-021-00703-0.
15. Grimaud, A., Diaz-Morales, O., Han, B., Hong, W.T., Lee, Y.-L., Giordano, L., Stoerzinger, K.A., Koper, M.T.M., and Shao-Horn, Y. (2017). Activating lattice oxygen redox reactions in metal oxides to catalyse oxygen evolution. Nat. Chem. *9*, 457–465. https://doi.org/10.1038/nchem.2695.
16. Pan, Y., Xu, X., Zhong, Y., Ge, L., Chen, Y., Veder, J.-P.M., Guan, D., O'Hayre, R., Li, M., Wang, G., et al. (2020). Direct evidence of boosted oxygen evolution over perovskite by enhanced lattice oxygen participation. Nat. Commun. *11*, 2002. https://doi.org/10.1038/s41467-020-15873-x.
17. Li, R., Liu, J., Xiao, M., Sun, Y., Liu, F., Gan, J., and Gao, S. (2024). Atomic Strain Wave-Featured LaRuIr Nanocrystals: Achieving Simultaneous Enhancement of Catalytic Activity and Stability toward Acidic Water Splitting. Small *20*, 2400095. https://doi.org/10.1002/smll.202400095.
18. Ping, X., Liu, Y., Zheng, L., Song, Y., Guo, L., Chen, S., and Wei, Z. (2024). Locking the lattice oxygen in RuO_2 to stabilize highly active Ru sites in acidic water oxidation. Nat. Commun. *15*, 2501. https://doi.org/10.1038/s41467-024-46815-6.
19. Hu, C., Yue, K., Han, J., Liu, X., Liu, L., Liu, Q., Kong, Q., Pao, C.-W., Hu, Z., Suenaga, K., et al. (2023). Misoriented high-entropy iridium ruthenium oxide for acidic water splitting. Sci. Adv. *9*, eadf9144. https://doi.org/10.1126/sciadv.adf9144.
20. Wu, Z.-Y., Chen, F.-Y., Li, B., Yu, S.-W., Finfrock, Y.Z., Meira, D.M., Yan, Q.-Q., Zhu, P., Chen, M.-X., Song, T.-W., et al. (2023). Non-iridium-based electrocatalyst for durable acidic oxygen evolution reaction in proton exchange membrane water electrolysis. Nat. Mater. *22*, 100–108. https://doi.org/10.1038/s41563-022-01380-5.
21. Han, X., Jin, M., Chen, T., Chou, T., Chen, J., Wang, S., Yang, Y., Wang, J., and Jin, H. (2024). Defect Engineering of RuO_2 Aerogel for Efficient Acidic Water Oxidation. ACS Mater. Lett. *6*, 748–755. https://doi.org/10.1021/acsmaterialslett.3c01414.

22. Deng, L., Hung, S.-F., Liu, S., Zhao, S., Lin, Z.-Y., Zhang, C., Zhang, Y., Wang, A.-Y., Chen, H.-Y., Peng, J., et al. (2024). Accelerated Proton Transfer in Asymmetric Active Units for Sustainable Acidic Oxygen Evolution Reaction. J. Am. Chem. Soc. *146*, 23146–23157. https://doi.org/10.1021/jacs.4c05070.

23. Kodera, M., Kawahara, Y., Hitomi, Y., Nomura, T., Ogura, T., and Kobayashi, Y. (2012). Reversible O–O Bond Scission of Peroxodiiron(III) to High-Spin Oxodiiron(IV) in Dioxygen Activation of a Diiron Center with a Bis-tpa Dinucleating Ligand as a Soluble Methane Monooxygenase Model. J. Am. Chem. Soc. *134*, 13236–13239. https://doi.org/10.1021/ja306089q.

24. Okamura, M., Kondo, M., Kuga, R., Kurashige, Y., Yanai, T., Hayami, S., Praneeth, V.K.K., Yoshida, M., Yoneda, K., Kawata, S., and Masaoka, S. (2016). A pentanuclear iron catalyst designed for water oxidation. Nature *530*, 465–468. https://doi.org/10.1038/nature16529.

25. Li, L., Zhang, G., Xu, J., He, H., Wang, B., Yang, Z., and Yang, S. (2023). Optimizing the Electronic Structure of Ruthenium Oxide by Neodymium Doping for Enhanced Acidic Oxygen Evolution Catalysis. Adv. Funct. Mater. *33*, 2213304. https://doi.org/10.1002/adfm.202213304.

26. Wang, Y., Yang, R., Ding, Y., Zhang, B., Li, H., Bai, B., Li, M., Cui, Y., Xiao, J., and Wu, Z.-S. (2023). Unraveling oxygen vacancy site mechanism of Rh-doped RuO_2 catalyst for long-lasting acidic water oxidation. Nat. Commun. *14*, 1412. https://doi.org/10.1038/s41467-023-37008-8.

27. Hao, S., Liu, M., Pan, J., Liu, X., Tan, X., Xu, N., He, Y., Lei, L., and Zhang, X. (2020). Dopants fixation of Ruthenium for boosting acidic oxygen evolution stability and activity. Nat. Commun. *11*, 5368. https://doi.org/10.1038/s41467-020-19212-y.

28. Du, K., Zhang, L., Shan, J., Guo, J., Mao, J., Yang, C.-C., Wang, C.-H., Hu, Z., and Ling, T. (2022). Interface engineering breaks both stability and activity limits of RuO_2 for sustainable water oxidation. Nat. Commun. *13*, 5448. https://doi.org/10.1038/s41467-022-33150-x.

29. Qin, Y., Yu, T., Deng, S., Zhou, X.-Y., Lin, D., Zhang, Q., Jin, Z., Zhang, D., He, Y.-B., Qiu, H.-J., et al. (2022). RuO_2 electronic structure and lattice strain dual engineering for enhanced acidic oxygen evolution reaction performance. Nat. Commun. *13*, 3784. https://doi.org/10.1038/s41467-022-31468-0.

30. Li, Q., Wang, D., Lu, Q., Meng, T., Yan, M., Fan, L., Xing, Z., and Yang, X. (2020). Identifying the Activation Mechanism and Boosting Electrocatalytic Activity of Layered Perovskite Ruthenate. Small *16*, 1906380. https://doi.org/10.1002/smll.201906380.

31. Jin, H., Liu, X., An, P., Tang, C., Yu, H., Zhang, Q., Peng, H.-J., Gu, L., Zheng, Y., Song, T., et al. (2023). Dynamic rhenium dopant boosts ruthenium oxide for durable oxygen evolution. Nat. Commun. *14*, 354. https://doi.org/10.1038/s41467-023-35913-6.

32. Deng, L., Hung, S.-F., Lin, Z.-Y., Zhang, Y., Zhang, C., Hao, Y., Liu, S., Kuo, C.-H., Chen, H.-Y., Peng, J., et al. (2023). Valence Oscillation of Ru Active Sites for Efficient and Robust Acidic Water Oxidation. Adv. Mater. *35*, 2305939. https://doi.org/10.1002/adma.202305939.

33. Zhang, D., Li, M., Yong, X., Song, H., Waterhouse, G.I.N., Yi, Y., Xue, B., Zhang, D., Liu, B., and Lu, S. (2023). Construction of Zn-doped RuO_2 nanowires for efficient and stable water oxidation in acidic media. Nat. Commun. *14*, 2517. https://doi.org/10.1038/s41467-023-38213-1.

34. Liu, G.-Q., Yang, Y., Zhang, X.-L., Li, H.-H., Yu, P.-C., Gao, M.-R., and Yu, S.-H. (2024). Porous Tellurium-Doped Ruthenium Dioxide Nanotubes for Enhanced Acidic Water Oxidation. Small *20*, 2306914. https://doi.org/10.1002/smll.202306914.

35. Liu, H., Zhang, Z., Fang, J., Li, M., Sendeku, M.G., Wang, X., Wu, H., Li, Y., Ge, J., Zhuang, Z., et al. (2023). Eliminating over-oxidation of ruthenium oxides by niobium for highly stable electrocatalytic oxygen evolution in acidic media. Joule *7*, 558–573. https://doi.org/10.1016/j.joule.2023.02.012.

36. Lee, K., Shim, J., Jang, H.Y., Lee, H.S., Shin, H., Lee, B.-H., Bootharaju, M. S., Lee, K.-S., Lee, J., Lee, S., et al. (2023). Modulating the valence electronic structure using earth-abundant aluminum for high-performance acidic oxygen evolution reaction. Chem *9*, 3600–3612. https://doi.org/10.1016/j.chempr.2023.08.006.

37. Moysiadou, A., and Hu, X. (2019). Stability profiles of transition metal oxides in the oxygen evolution reaction in alkaline medium. J. Mater. Chem. A *7*, 25865–25877. https://doi.org/10.1039/C9TA10308B.

38. Łukaszewski, M., and Czerwiński, A. (2006). Dissolution of noble metals and their alloys studied by electrochemical quartz crystal microbalance. J. Electroanal. Chem. *589*, 38–45. https://doi.org/10.1016/j.jelechem.2006.01.007.

39. Sauerbrey, G., and Sauerbrey, G.Z. (1959). The use of quarts oscillators for weighing thin layers and for microweighing. Eur. Phys. J. A *155*, 206–222.

40. Li, P., Wang, M., Duan, X., Zheng, L., Cheng, X., Zhang, Y., Kuang, Y., Li, Y., Ma, Q., Feng, Z., et al. (2019). Boosting oxygen evolution of single-atomic ruthenium through electronic coupling with cobalt-iron layered double hydroxides. Nat. Commun. *10*, 1711. https://doi.org/10.1038/s41467-019-09666-0.

41. Zhu, W., Song, X., Liao, F., Huang, H., Shao, Q., Feng, K., Zhou, Y., Ma, M., Wu, J., Yang, H., et al. (2023). Stable and oxidative charged Ru enhance the acidic oxygen evolution reaction activity in two-dimensional ruthenium-iridium oxide. Nat. Commun. *14*, 5365. https://doi.org/10.1038/s41467-023-41036-9.

42. Chen, D., Yu, R., Yu, K., Lu, R., Zhao, H., Jiao, J., Yao, Y., Zhu, J., Wu, J., and Mu, S. (2024). Bicontinuous RuO2 nanoreactors for acidic water oxidation. Nat. Commun. *15*, 3928. https://doi.org/10.1038/s41467-024-48372-4.

43. Zhu, W., Yao, F., Cheng, K., Zhao, M., Yang, C.-J., Dong, C.-L., Hong, Q., Jiang, Q., Wang, Z., and Liang, H. (2023). Direct Dioxygen Radical Coupling Driven by Octahedral Ruthenium–Oxygen–Cobalt Collaborative Coordination for Acidic Oxygen Evolution Reaction. J. Am. Chem. Soc. *145*, 17995–18006. https://doi.org/10.1021/jacs.3c05556.

44. Hao, Y., Hung, S.-F., Zeng, W.-J., Wang, Y., Zhang, C., Kuo, C.-H., Wang, L., Zhao, S., Zhang, Y., Chen, H.-Y., and Peng, S. (2023). Switching the Oxygen Evolution Mechanism on Atomically Dispersed Ru for Enhanced Acidic Reaction Kinetics. J. Am. Chem. Soc. *145*, 23659–23669. https://doi.org/10.1021/jacs.3c07777.

45. Wang, X., Chen, J., Zeng, J., Wang, Q., Li, Z., Qin, R., Wu, C., Xie, Z., and Zheng, L. (2017). The synergy between atomically dispersed Pd and cerium oxide for enhanced catalytic properties. Nanoscale *9*, 6643–6648. https://doi.org/10.1039/C6NR09707C.

46. Kibis, L.S., Simanenko, A.A., Stadnichenko, A.I., Zaikovskii, V.I., and Boronin, A.I. (2021). Probing of Pd4+ Species in a PdO_x–CeO_2 System by X-Ray Photoelectron Spectroscopy. J. Phys. Chem. C *125*, 20845–20854. https://doi.org/10.1021/acs.jpcc.1c04646.

47. Xu, J., Jin, H., Lu, T., Li, J., Liu, Y., Davey, K., Zheng, Y., and Qiao, S.-Z. (2023). $IrO_x{\cdot}nH_2O$ with lattice water ssisted oxygen exchange for high-performance proton exchange membrane ater electrolyzers. Sci. Adv. *9*, eadh1718. https://doi.org/10.1126/sciadv.adh17.

48. Gauthier, J.A., Dickens, C.F., Chen, L.D., Doyle, A.D., and Nørskov, J.K. (2017). Solvation Effects for Oxygen Evolution Reaction Catalysis on IrO_2(110). J. Phys. Chem. C *121*, 11455–11463. https://doi.org/10.1021/acs.jpcc.7b02383.

49. Dickens, C.F., Montoya, J.H., Kulkarni, A.R., Bajdich, M., and Nørskov, J. K. (2019). An electronic structure descriptor for oxygen reactivity at metal and metal-oxide surfaces. Surf. Sci. *681*, 122–129. https://doi.org/10.1016/j.susc.2018.11.019.